Electronic Supplementary Material (ESI) for Soft Matter.

Scaling mechanical instabilities in drying micellar droplets

Jayant K Dewangan,[a] Nandita Basu[b] and Mithun Chowdhury[a,*]

[a]Lab *of* Soft Interfaces, Department of Metallurgical Engineering and Materials Science, Indian Institute of Technology Bombay, Mumbai 400076, India

[b]Department of Chemistry, Indian Institute of Technology Bombay, Mumbai 400076, India

*correspondence to: mithunc@iitb.ac.in (MC)

Electronic Supplementary Information (ESI)

List of movies

M1	C_{CTAB} of 3.64 wt% aqueous droplet drying at T_S = 90 °C on the glass substrate and radial wrinkling
M2	C_{CTAB} of 3.64 wt% aqueous droplet drying at T_S = 90 °C on the cross-linked PDMS substrate and Rayleigh–Bénard instability development
M3	C_{CTAB} of 1.82 wt% aqueous droplet drying at T_S = 90 °C on the glass substrate and double radial wrinkling

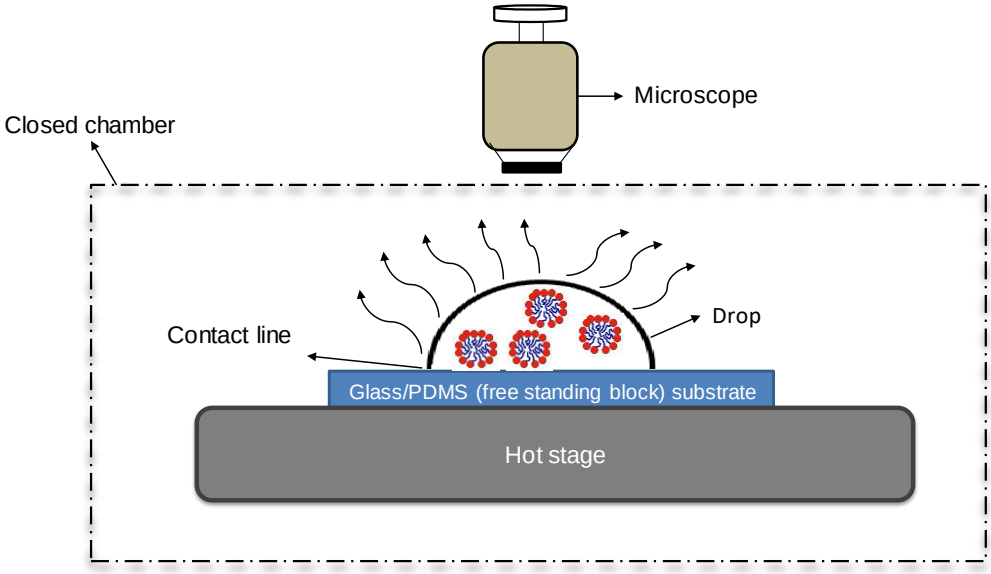

Figure S1: Schematic presentation of evaporative drying of CTAB containing droplets placed on a hot substrate where the temperature of the substrate is maintained at a fixed value, T_S.

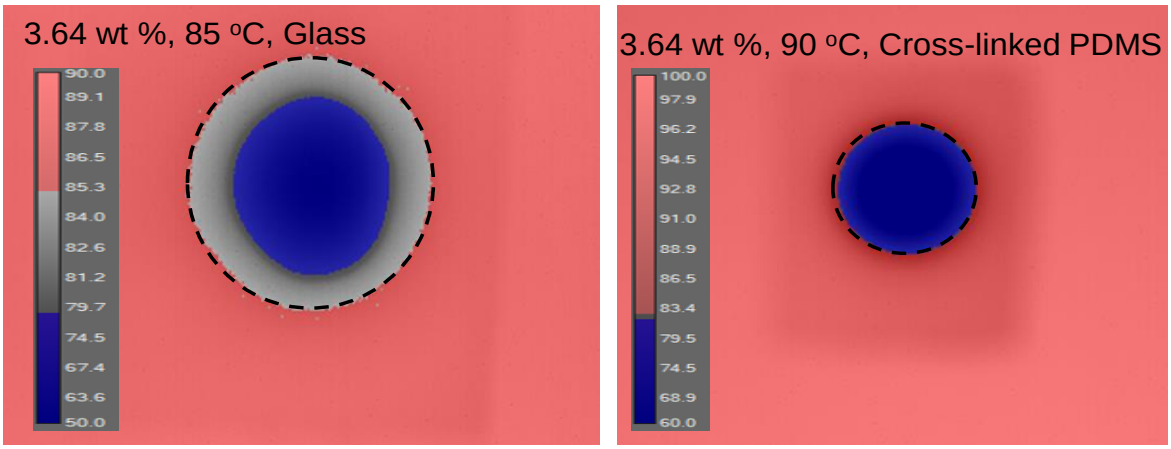

Figure S2: Infrared (IR) thermography of the micellar droplets (3.64 wt %) placed on a (a) glass substrate and (b) cross-linked PDMS substrate where both the substrates are kept on a hot stage which is maintained at temperatures 90 °C and 100 °C, resulting temperature of droplet bases as 85 °C and 90 °C, respectively. The droplet bases are pointed by dotted black circles. The temperature across the contact line is uniformly distributed and same as the temperature of the droplet base. Temperature difference between the droplet base and apex is significant on low energy cross-linked PDMS substrate as compared to high energy glass substrate.

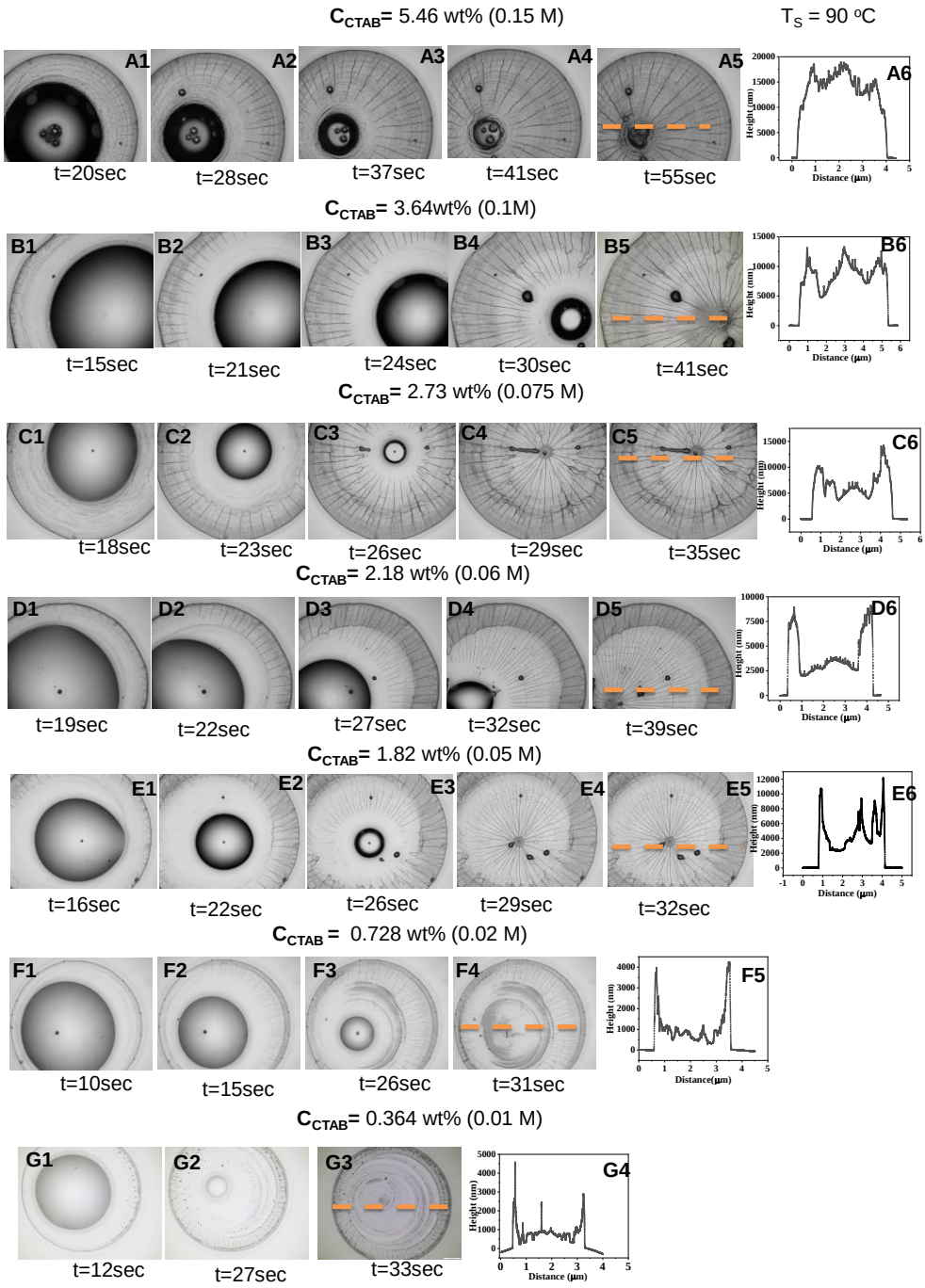

Figure S3: Real-time optical micrographs showing the nucleation and propagation of radial wrinkles on rigid glass substrate during evaporation-driven drying of CTAB containing aqueous micellar solution droplets of different concentrations (C_{CTAB}) at T_S = 90 ºC. The initial concentrations used for the real-time study includes (A1-A5): 5.46 wt% (0.15 M), (B1-B5): 3.64wt% (0.1M), (C1-C5): 2.73 wt% (0.075 M), (D1-D5): 2.18 wt% (0.06 M), (E1-E5) 1.82 wt% (0.05 M), (F1-F4) 0.728 wt% (0.02 M), (G1-G3) 0.364 wt% (0.01 M). (A6, B6, C6, D6, E6, F5, and G4 show the height profiles across the deposits for the dotted yellow lines drawn on the deposit images shown in frames A5, B5, C5, D5, E5, F4, and G3. The size of each micrograph is 3.4 mm x 2.8 mm.

Influence of substrate temperature on the resulting surface wrinkling patterns

The surface wrinkling patterns are visible at different substrate temperatures T_S. For the ease of the discussion, we classify our substrate temperatures (T_S) into two ranges as the wrinkle morphologies appear closely similar at the temperatures within the mentioned temperature ranges. (1) $T_S \leq 75$ ^oC (2) $T_S > 75$ ^oC

On the glass substrate

At C_{CTAB} = 0.364 wt%, at $T_S \leq 75$ ^oC, deposits comprise a few cracked stick-slip regimes and significantly thick peripheral rings (see Figure S6a1). At $T_S > 75$ ^oC the gel-like film spreads over a wider inward area, resulting in reticular type wrinkle morphology over a wider region. As a result, the number of stick-slip regimes lowers (see Figure S4a2). We have noticed that at ca. $T_S \geq 85$ ^oC, a transition from reticular to radial wrinkles occurs at the pinned deposit rim, propagating certain distances depending on C_{CTAB}. The poor contrast in the interior containing stick-slip regimes indicates that the film thickness in the region is significantly low (see Figure S4a3). A closer look through FESEM reveals that these regions comprise blister-like morphologies that appear directionally opposite the radial wrinkles (Figure S7a3). Deposits that arise at $T_S > 90$ ^oC are seen to be devoid of any stick-slip regime in the central part. As a result, we see a much wider peripheral zone with largely-spaced radial wrinkles (see Figure S4a4). At $T_S = 90$ ^oC with increase in C_{CTAB} to 0.728 wt% L (wrinkle length) increases. Due to the reduced film thickness in the interior of the deposits, the radial wrinkles stop propagating, giving rise to directionally opposite (frames d and d1 of Figure 2) closely-spaced blister-like morphology much denser as compared to what we observed for C_{CTAB} = 0.364 wt% (Figure S7b3). At $T_S \leq 75$ ^oC instead of stick-slip regimes (as observed for C_{CTAB} = 0.364 wt%), few cracks are observed over the nearly uniform middle to central deposit morphologies along with thick peripheral rings (see Figure S4b1). At $T_S = 85$ ^oC, reticular type wrinkles at the edge and blister-like wrinkling morphology in the interior are observed (Figure S4b2), which gets converted to radial wrinkles when T_S reaches a value of 90 ^oC (Figure S4b3). Interestingly, at a sufficiently high T_S of 100 ^oC, the peripheral regions are seen to contain few radial wrinkles of much lower length than obtained at $T_S = 90$ ^oC. In this case, reticular wrinkles are observed through the whole deposit area (see Figure S4b4).

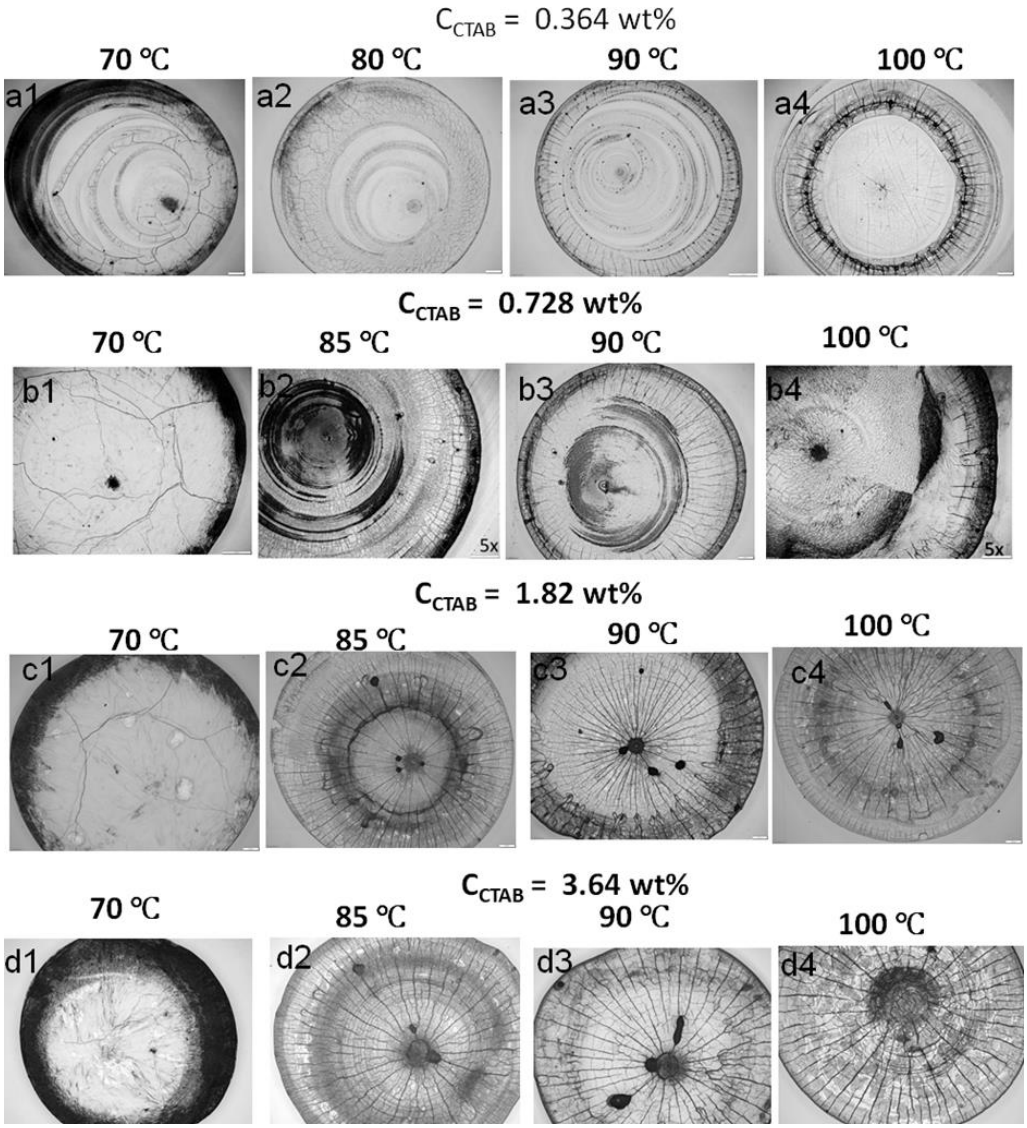

Figure S4: Various cracks and wrinkling morphologies over a wide range of substrate temperatures, T_S with different C_{CTAB} on glass substrates. Size of each image is 3.4 mm x 2.8 mm

Cracked films are obtained at $T_S \leq 75$ °C for $C_{CTAB} \geq 1.82$ wt%. The number of cracks decreases with an increase in C_{CTAB} (Figures S6 c1, d1). At $C_{CTAB} \geq 1.82$ wt% beyond T_S of 85 °C, radial wrinkles are observed all over the deposits (see frames c2, c3, c4 and d2, d3, d4 of Figure S6).

On the cross-linked PDMS substrate

At $T_S \leq 75$ °C, deposits formed from the evaporative droplet of $C_{CTAB} \leq 0.728$ wt% contain a thick outer ring without any wrinkling morphology. It accompanies a central area that remains almost devoid of any deposition (frames a1, b1 of Figure S6). FESEM images reveal (see Figure S7a) an increased micellar length attributed to the transformation of spherical

micelles into rod-like micelles facilitated at high temperatures. We can see from the frames b, c,d of Figures S5 that the rod-like micelles get wider with the increase in C_{CTAB} at T_S = 75 ^oC.

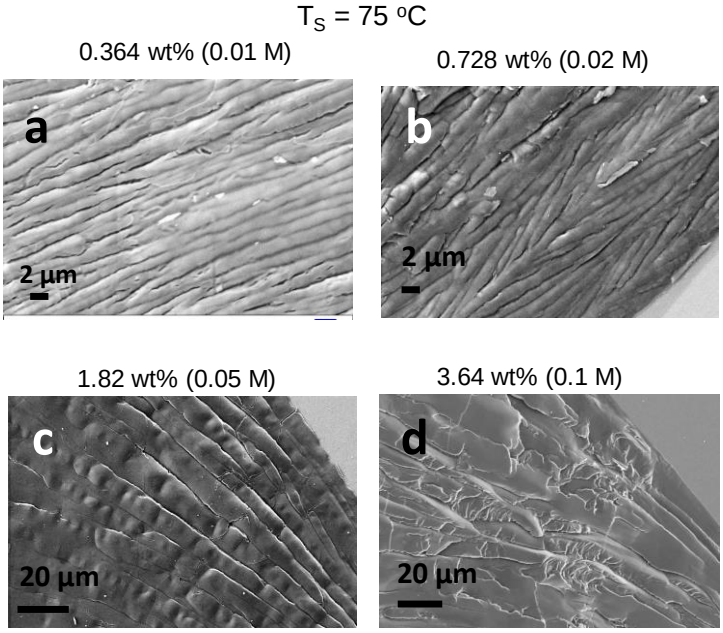

Figure S5: Rod-like micelles appear at various C_{CTAB} at T_S = 75 ^oC.

At T_S > 75 ^oC, an undulated peripheral edge is observed. When T_S reaches a value of 90 ^oC, the extent of deformation of cross-linked PDMS substrate gets enhanced, leading to circular wrinkles formation, as can also be seen from the frames i and i1 of Figure 2. At a slightly higher C_{CTAB} to 0.728 wt%, in the temperature range, $T_s \leq 75$ ^oC, extremely thick peripheral rings are observed in the obtained deposits without any wrinkle formation. At $T_s \geq 75$ ^oC relatively wider region gets wrinkled (frames b2, b3 of Figure S6). Further increase in C_{CTAB}, the thickness of the peripheral film significantly reduces, leading to a thicker interior without any sign of surface wrinkling (frame c2 of Figure S6). Circular wrinkle formation gets initiated at T_S = 90 ^oC with an even larger width of the wrinkled region (see Figure 2). At T_S = 95 ^oC, the width of the circularly wrinkled zone increases (frame c3 of Figure S6). Interestingly at a much higher value of C_{CTAB} of 3.64 wt% (0.1 M), the deposits obtained at $T_S \leq 75$ ^oC encounter a double deposit, i.e., a central zone appears, which remains utterly devoid of any material closely looking like a cavity (frame d1 of Figure S6). Interestingly, At T_S = 85 ^oC, the whole deposit gets buckled (see frame d2 of Figure S6), which is converted into closely-spaced circular wrinkles once the T_S reaches the value of 90 ^oC (see frame d3 of Figure S6).

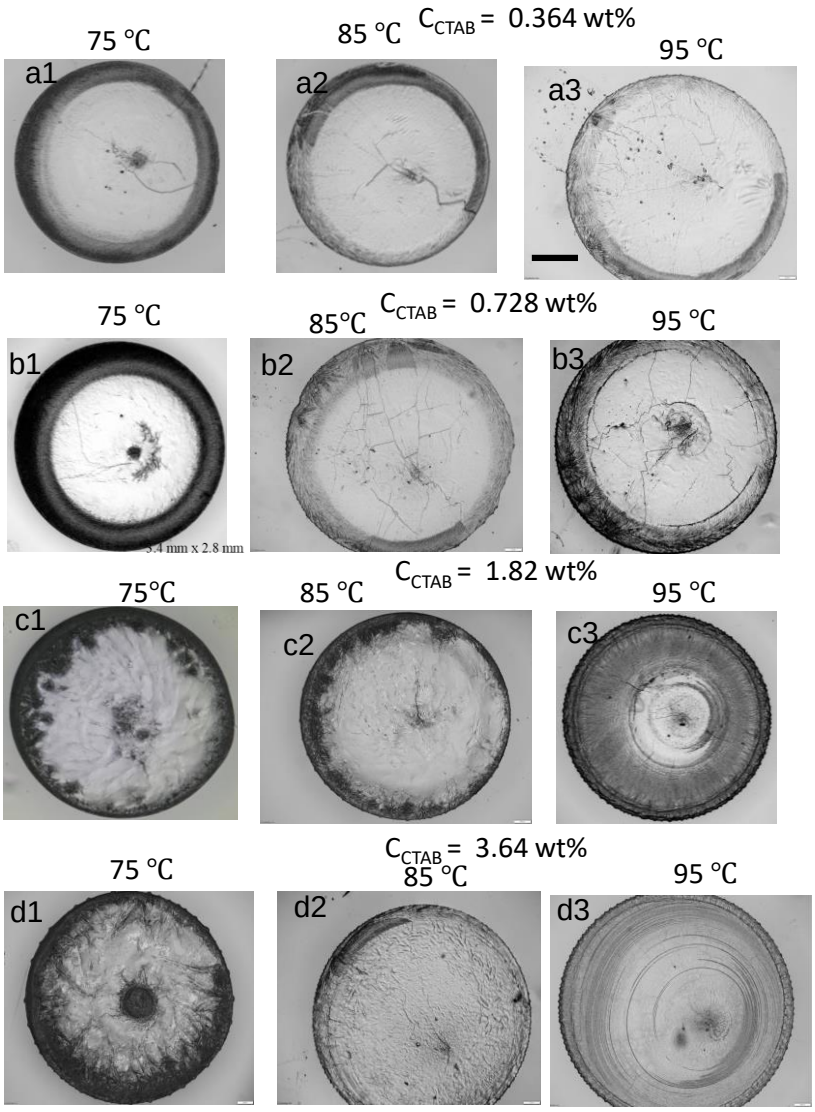

Figure S6: Various cracks and wrinkling morphologies over a wide range of substrate temperatures, T_S with different C_{CTAB} on cross-linked PDMS substrates. Size of the scale bar in a3 is 500 μm and it is applicable to all other micrographs.

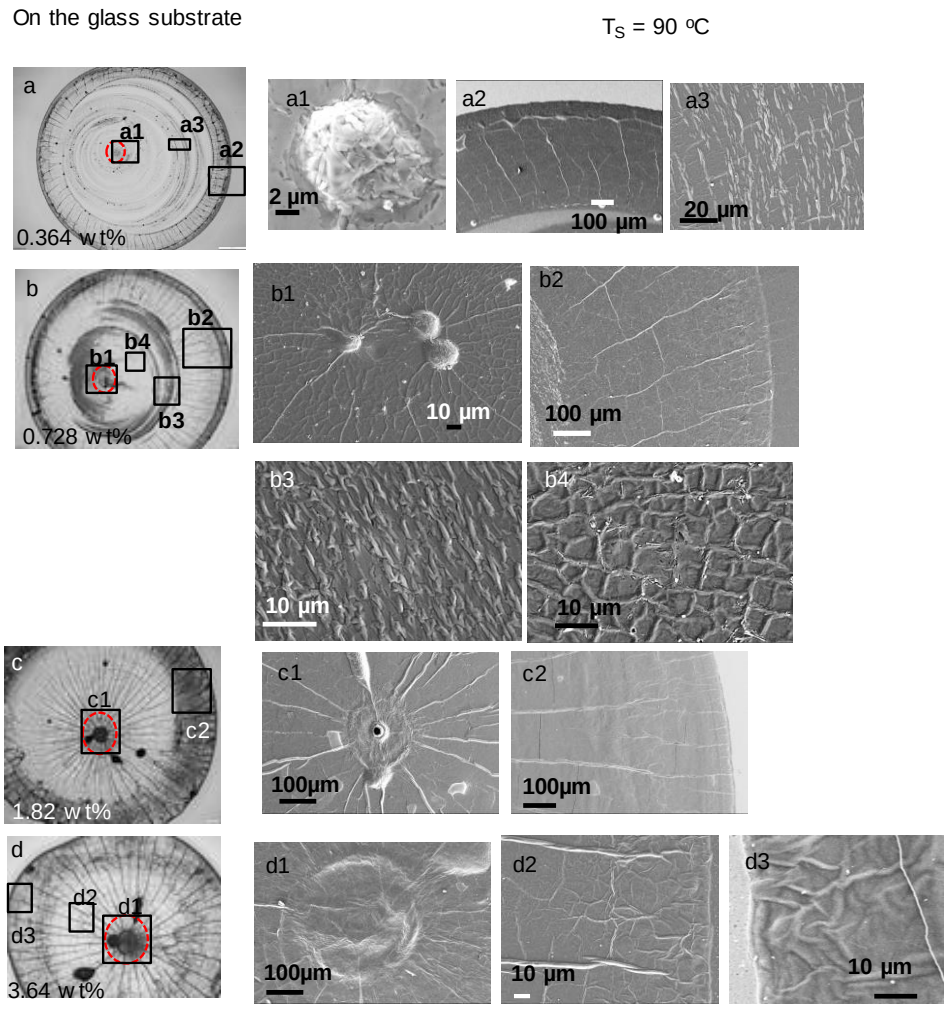

Figure S7: (a1, b1, c1, d1) The detailed morphology of the central regions indicated by the red dotted circles are shown through FESEM micrographs. The area of these centrally buckled regions increases with C_{CTAB}. FESEM images show radial wrinkles (a2, b2, c2, d2), blister-like wrinkles (a3, b3), and reticular–type wrinkles (b4). The wrinkled area between two radial wrinkles is visible in (d3). Each (a, b, c, d) is 3.4 mm x 2.8 mm in size.

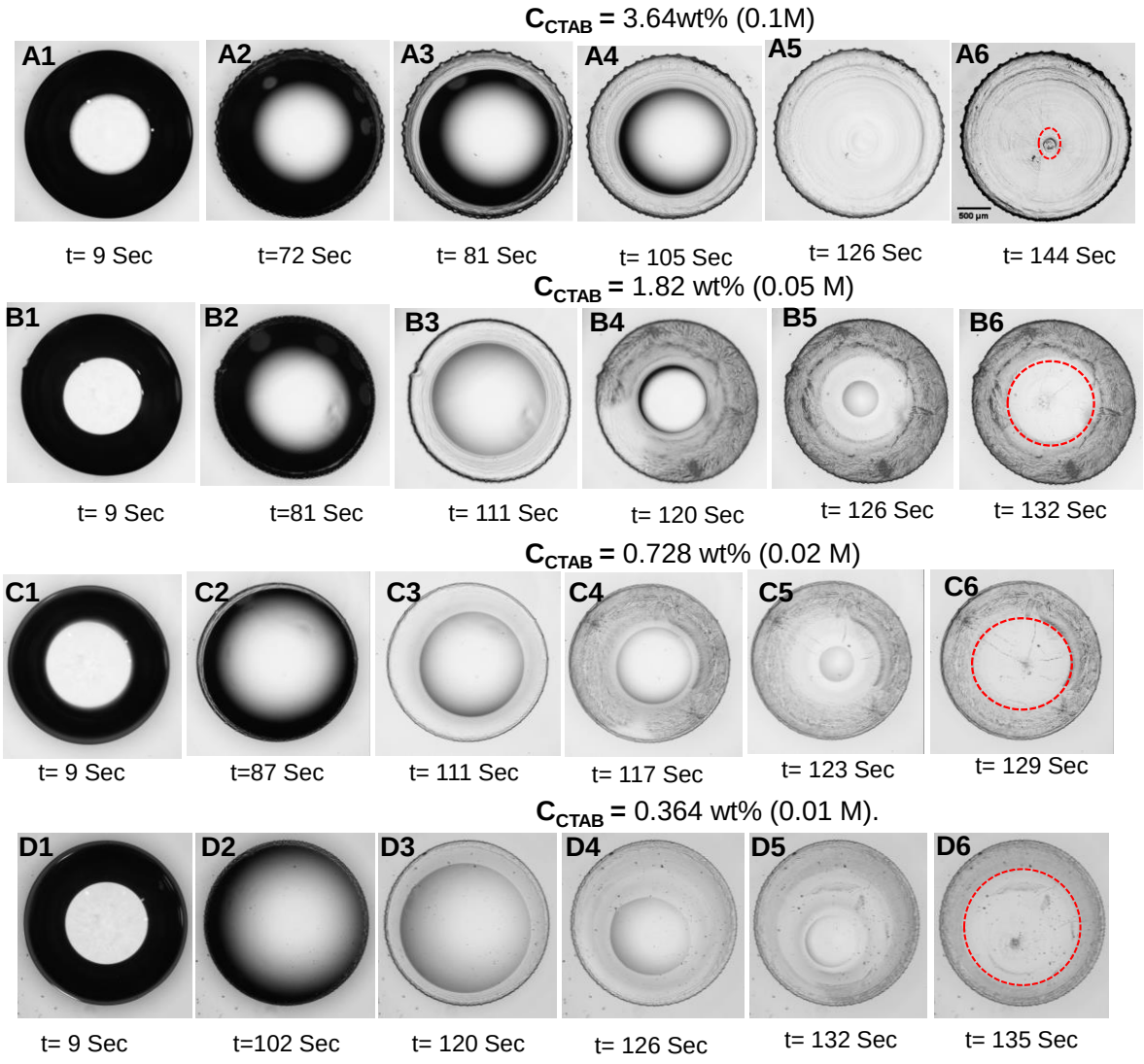

Figure S8: Real-time optical micrographs showing the nucleation and propagation of close-to circular wrinkles on cross-linked PDMS substrate during evaporation-driven drying of CTAB containing aqueous micellar solution droplets of different concentrations (C_{CTAB}) at T_S = 90 °C. The initial concentrations used for the real-time study includes (A1-A6) 3.64 wt% (0.1 M), (B1-B6) 1.82 wt% (0.05 M), (C1-C6) 0.728 wt% (0.02 M), (D1-D6) 0.364 wt% (0.01 M). The size of the scale bar in A6 is 500 μm and it is applicable to each of the micrographs.

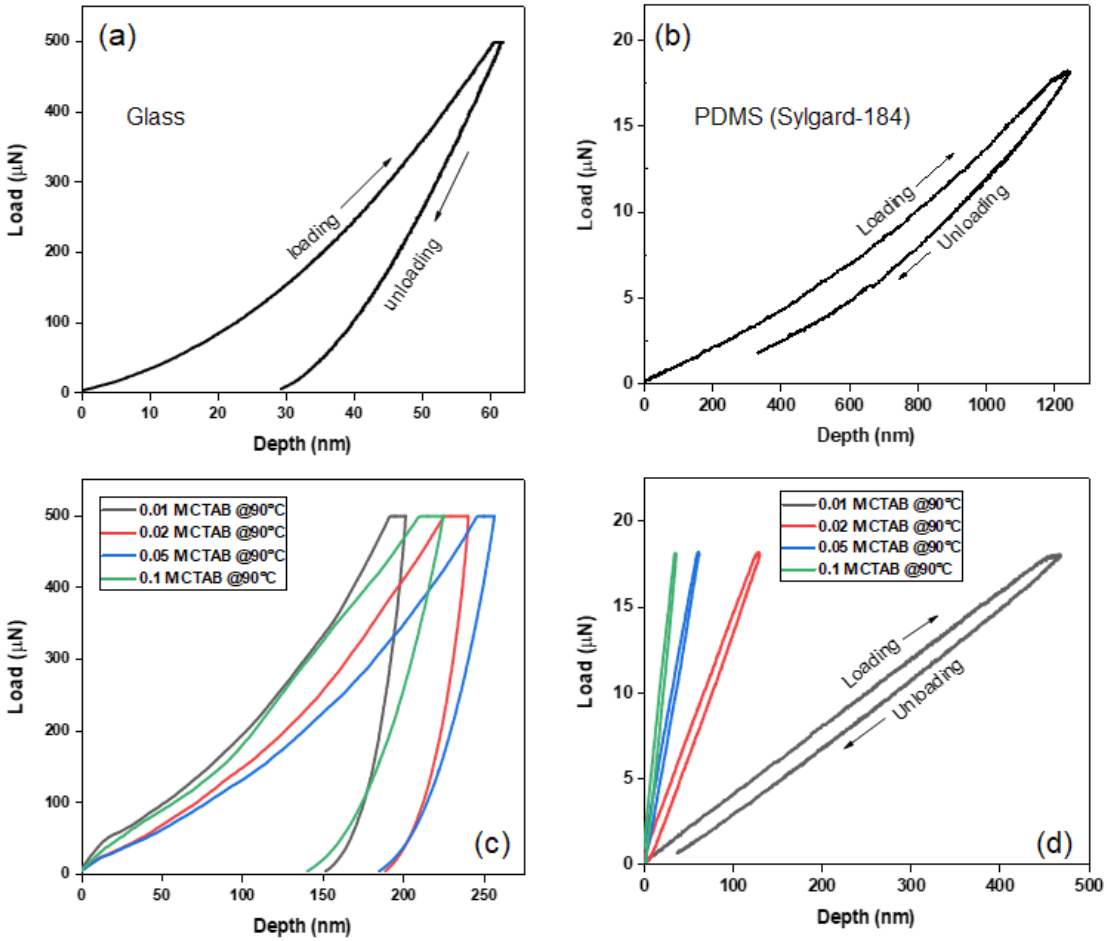

Figure S9: Load-displacement curves during nanoindentation for (a) glass substrate (b) cross-linked PDMS substrate (c) dried deposit on the glass substrate (d) dried deposit on cross-linked PDMS substrate.

Table S1: Values of exponents obtained by fitting the data with φ^n on rigid glass substrate at various T_S

Glass substrate temperature (T_s)	$\frac{w}{R} \sim \varphi^n$
40 °C	$\sim \varphi^{0.42 \pm 0.01}$
60 °C	$\sim \varphi^{0.46 \pm 0.02}$
75 °C	$\sim \varphi^{0.42 \pm 0.04}$
85 °C	$\sim \varphi^{0.42 \pm 0.06}$
90 °C	$\sim \varphi^{0.41 \pm 0.04}$
95 °C	$\sim \varphi^{0.38 \pm 0.06}$

.

Table S2: Values of exponents obtained by fitting the data with φ^n on soft cross-linked PDMS substrate at various T_S

PDMS substrate temperature (T_s)	$\frac{w}{R} \sim \varphi^n$
40 °C	$\sim \varphi^{0.29 \pm 0.02}$
60 °C	$\sim \varphi^{0.27 \pm 0.02}$
75 °C	$\sim \varphi^{0.38 \pm 0.04}$
85 °C	$\sim \varphi^{0.48 \pm 0.06}$
90 °C	$\sim \varphi^{0.40 \pm 0.03}$